AIAA SciTech Forum
6-10 January 2020, Orlando, FL
AIAA Scitech 2020 Forum

10.2514/6.2020-1368

Separation Control Inside a Rectangular Supersonic Inlet Using Dielectric Barrier Discharge Plasma Actuators

Christian Porrello * and Subrata Roy †
University of Florida, Gainesville, FL, 32611

Rogerio Pimentel ‡
Defence Research and Development Canada, Valcartier Research Centre, QC, Canada, G3J 1X5

A parametric 2D computational fluid dynamics (CFD) study of flow control within a supersonic air inlet using surface dielectric barrier discharge (SDBD) plasma actuators was performed. The objective of this study was to establish receptive locations and orientations for the SDBD actuators where the actuator effects would be most pronounced and to assess the potential for SDBD actuators to increase the total pressure recovery and decrease the total pressure distortion of a rectangular supersonic inlet in Mach 2.5 flight. Linear plasma actuators were modelled as a time-averaged body force. Ultimately, 2D results demonstrated limited influence on the supersonic flow within the inlet across all locations, orientations, and actuator strengths tested for linear actuators which apply their force primarily in the streamwise direction. Based on the results, 3D CFD simulations of different actuator geometries are planned for the future direction of the current research.

Nomenclature

P_0	=	mean total pressure at the face of the combustor
P	=	total pressure
f	=	directional component of plasma forcing model
F_0	=	time-averaged electrodynamic force constant
β	=	dielectric material factor for plasma forcing model
x_0	=	midpoint of plasma actuator location in the x direction
y_0	=	midpoint of plasma actuator location in the y direction
A	=	constant gain factor for plasma forcing function
M	=	Mach number
T	=	stagnation temperature

*Undergraduate Student, Applied Physics Research Group, AIAA Student Member.
†Professor, Applied Physics Research Group, AIAA Associate Fellow
‡Defence Scientist, Weapons Systems Section

Δt = time step used for transient simulations

Subscripts

∞ = freestream condition

x = component in the horizontal $\hat{x}$ direction for 2D CFD simulations

y = component in the vertical $\hat{y}$ direction for 2D CFD simulations

I. Introduction

The objective of an air inlet is to bring the freestream flight conditions to the operating conditions required by the combustor. Optimally, the air inlet should deliver a uniform, subsonic air supply at high pressure to the combustor. However, the design of supersonic air inlets is complicated due to the presence of shocks. Supersonic inlets generate a series of oblique shock waves followed by a terminal normal shock wave and adverse pressure gradient. The shock wave/boundary layer interactions (SBLI) within the inlet will cause rapid thickening and separation of the boundary layer [1], and if unmanaged the low-energy boundary layer may decrease the performance and stability of the engine. To manage the SBLI, supersonic inlet designs have traditionally used diverter splitter plates to separate the main air intake from the separating boundary layer or bleed systems to ingest the boundary layer from the ingested airstream. However, these solutions add to the weight, drag, complexity, cost, and maintenance requirements of the inlet because of the mechanical components involved [2]. Consequently, there is interest in improving the performance of supersonic inlets using simpler systems. The present work focuses on the 2D computational fluid dynamics (CFD) simulation of a rectangular supersonic inlet at zero angle-of-attack (AOA) with active flow control using surface dielectric barrier discharge (SDBD) non-thermal plasma actuators. The objective of this work is to establish the feasibility of flow control for improved performance of a supersonic inlet using DBD actuators across several plasma actuator orientations, locations, and strengths.

Recent work demonstrates the potential for DBD actuators in active flow control at supersonic speeds [3–7]. Over other methods of active flow control, plasma actuators are faster, lightweight, lack moving components, low power, and widely applicable [8]. For the SDBD actuators considered in the present work, induced velocities of 5-10 m/sec are reasonable [8]. At these speeds, DBD actuators have been shown to influence the turbulent boundary layer of supersonic flow, showing potential for DBD flow control within supersonic inlets [3]. Indeed, several comparable works to the current study demonstrate this potential [4–7]. However, these studies focus on different inlet designs, plasma actuator types, or specific actuator locations. Therefore, there is a need for a parametric study on this subject matter where receptive SDBD actuator locations and orientations are identified and the influence of actuator strength is described. Our research aims to assess the effectiveness of SDBD actuators to improve the performance of supersonic air inlets.

This paper is organized as follows. Section II briefly describes the inlet performance parameters of interest to this work and Section III describes the numerical methodology and plasma model used in the 2D CFD simulations. Then, Section IV summarizes the preliminary results obtained and Section V provides concluding remarks and describes the future direction of this research.

II. Relevant Inlet Performance Parameters

This section briefly describes the inlet performance parameters relevant to this work: inlet total pressure recovery and inlet total pressure distortion at the pitot rake station in Fig. 1. There are many other additional performance parameters that should be considered in the complete design of an inlet such as weight, drag, noise, stealth, and cost. However, these performance parameters are outside the scope of this work.

A. Pressure Recovery

In general, there are considerable pressure losses as the supersonic inlet brings the freestream to subsonic speeds to match the requirements of the engine. These pressure losses are partly described by the pressure recovery of the inlet which states the mean total pressure at a plane in front of the combustor face as a fraction of the freestream total pressure:

$$\text{total pressure recovery} = \frac{P_0}{P_\infty} \tag{1}$$

For subsonic speeds, a rule of thumb states that for every 1% decrease in the pressure recovery of the inlet, there is at least a 1% increase in thrust loss for the engine [9]. However, the consequences for lower pressure recovery increase for supersonic flight. For example, an 8% decrease in pressure recovery will cost the typical engine a 13% decrease in thrust and 5% increase in fuel consumption [10]. Consequently, the ideal inlet design maximizes pressure recovery from the freestream.

B. Inlet Pressure Distortion

In addition to delivering high pressure recovery from the freestream, the inlet must deliver an air supply with a uniform pressure distribution. This pressure distribution is described by the inlet total pressure distortion which could be calculated as:

$$\text{total pressure distortion} = \frac{P_{0,\max} - P_{0,\min}}{P_\infty} \tag{2}$$

High pressure distortions indicate large pressure fluctuations in the compression system which decrease the combustion stability and may lead to blade fatigue and/or decreased engine efficiency [8]. Furthermore, high pressure distortions may increase the chance of compression surge in which event there is a complete loss of thrust [11]. Consequently, the ideal inlet design minimizes pressure distortion in the face of the combustor.

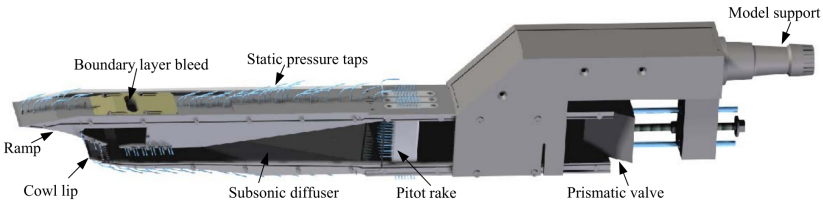

Fig. 1 The wind tunnel model from which the 2D CFD geometry is modelled. In order to vary the back-pressure for simulating different operating conditions of the combustor, a prismatic valve is positioned at the end of a straight channel. Note that the end of the air inlet coincides with the pitot rake station [12].

III. Methodology

A. Geometry and Numerical Mesh

For this work, the commercial CFD software ANSYS Fluent (Version 19.2) is used to perform a parametric 2D study of a rectangular supersonic inlet at zero AOA with and without plasma actuators. The geometry for this work was adopted from the experimental setup described in Ref. [12] as shown in Fig. 1. The insertion depth of the prismatic valve at the exit of the inlet is 20.57 mm. For the CFD simulations, an unstructured mesh of approximately 900K elements was used. At each wall in the mesh, the mesh is refined in the wall normal direction with the smallest mesh spacing of $y^+ < 1$ as shown in Fig. 2.

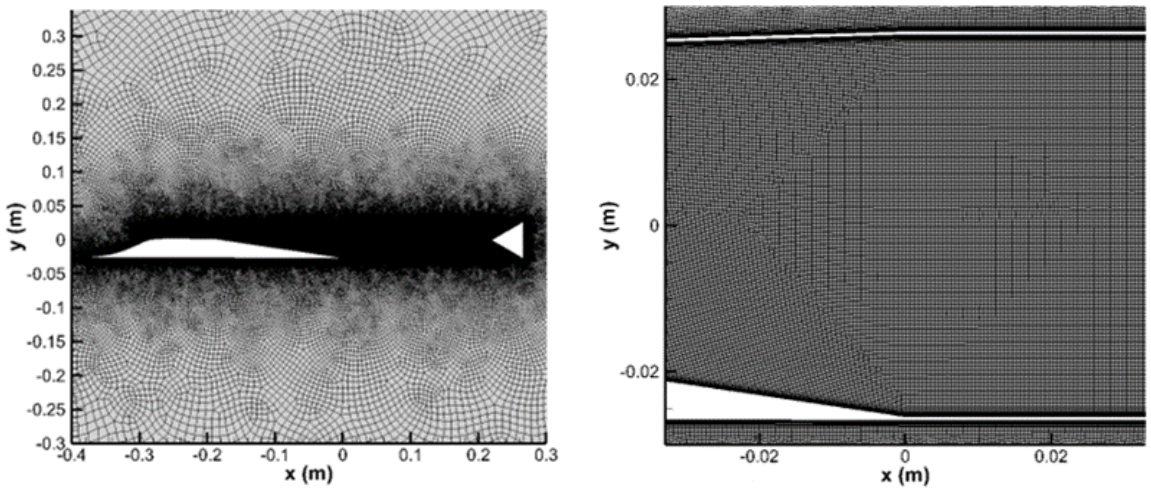

(a) (b)

Fig. 2 2D mesh used for CFD simulations zoomed to highlight the (a) the air inlet and straight channel and (b) the end of the inlet which coincides with the line $x = 0$. A finite wall thickness of 1 mm was used where applicable. All corners were rounded with the exception of the prismatic valve which was left sharp. Lastly, the mesh geometry was flipped from the experimental setup shown in Fig. 1.

B. Numerical Method

For this study, Fluent's second-order explicit coupled pressure-velocity solver was used to numerically solve the compressible Navier-Stokes equations in 2D [13]:

$$\frac{\partial}{\partial t}\Big(\rho\Big) + \nabla \cdot (\rho \mathbf{u}) = 0 \tag{3}$$

$$\frac{\partial}{\partial t}\Big(\rho \mathbf{u}\Big) + \nabla \cdot \Big[\rho \mathbf{u}\mathbf{u} + p\mathbf{I} - \tau\Big] = \mathbf{f} \tag{4}$$

$$\frac{\partial}{\partial t}\Big(\rho E\Big) + \nabla \cdot \Big[(\rho E + p)\mathbf{u} + \mathbf{q} - \mathbf{u} \cdot \tau\Big] = \mathbf{u} \cdot \mathbf{f} \tag{5}$$

First, a CFD simulation without any plasma actuators was performed to establish a benchmark for simulations with plasma actuators. A pressure far-field outer boundary condition (BC) was used to impose the freestream conditions reported in Table 1, and the fluid domain was initialized with those conditions. Turbulence was incorporated into the simulation using the Spalart-Allmaras turbulence model with curvature correction. A convergence criteria of 10^{-3} for the scaled residuals of the continuity, $\hat{x}$ momentum and $\hat{y}$ momentum equations was imposed. For the scaled residuals of the total energy and turbulent kinetic energy equations, a convergence criteria of 10^{-6} was imposed. Lastly, the air density was computed using the ideal gas law and the fluid viscosity was computed from Sutherland's law.

Subsequently, a parametric study with plasma actuators was performed to determine suitable plasma actuator locations, orientations, and actuator strengths. Each simulation was initialized using the results from a simulation without plasma actuators and was solved using the same solver controls. Due to the large number of simulations required, each simulation was performed on a reduced mesh of approximately 400K elements. The reduced mesh was found to capture the salient features of the flow and the calculated mass flow rate (0.168 kg/s), flow distortion (76.57 %), and pressure recovery (48.31 %) were within reasonable agreement to experimental results as shown in Table 3. Subsequently, a set of transient simulations was performed on the finer mesh. A time step of $\Delta t = 2$ ms was used to advance the solution in time.

Table 1 Supersonic Freestream Conditions

Quantity	Value
M_∞	2.5
P_∞	100 kPa
T_∞	297 K

C. Plasma Actuator Model

For this work, plasma actuators were implemented in 2D as a time-averaged body force term following the exponential body force model described by Ref. [14]:

$$f_x = \mathrm{A}\frac{F_{x,0}}{\sqrt{F_{x,0}^2 + F_{y,0}^2}} \exp\left(-\left(\frac{(x - x_0) - (y - y_0)}{y - y_0 + y_b}\right)^2 - \beta_x (y - y_0)^2 \right) \tag{6}$$

$$f_y = \mathrm{A}\frac{F_{y,0}}{\sqrt{F_{x,0}^2 + F_{y,0}^2}} \exp\left(-\left(\frac{(x - x_0)}{y - y_0 + y_b}\right)^2 - \beta_y (y - y_0)^2 \right) \tag{7}$$

In Eq. (6) and Eq. (7), the values of $F_{x,0}$ and $F_{y,0}$ are constants found by solving for the average electrodynamic force from air-plasma equations. The constants β_x and β_y are properties of the dielectric material used for the DBD plasma actuator [14]. Values for these constants are taken from Ref. [15] and their values are reported in Table 2. For this work, an additional amplifying factor A was introduced to modulate the strength of the forcing function. Although this exponential model lacks the accuracy of direct simulation of the plasma physics involved, direct simulation of the plasma physics is non-trivial for supersonic flows. The model is much more computationally efficient and sufficiently accurate for this study [16].

Table 2 Plasma Actuator Forcing Function Constants

Quantity	Value
F_x	2.6
F_y	2.0
β_x	1.44×10^5
β_y	1.8×10^6
y_b	1.665×10^{-3}

IV. Results

A. Flow without Plasma Actuators

After approximately 350 iterations, the steady-state coupled pressure-velocity solver converged to a solution for flow in the inlet without any plasma actuators. Figure 3 shows contours of the Mach number in the inlet. For this prismatic valve insertion depth, the results demonstrate an improperly started air inlet. A standing normal shockwave prevents a compression wave system from forming at the cowl lip as shown in Fig. 4. Also shown in Fig. 4 is a separating boundary layer developing on the ramp. Without any method to remove or manage the separating boundary layer, Fig. 3 demonstrates that the flow detaches from the ramp at the diffuser. The result is a large region of supersonic flow and a non-uniform total pressure profile at the exit of the inlet and combustor face shown in Fig. 5.

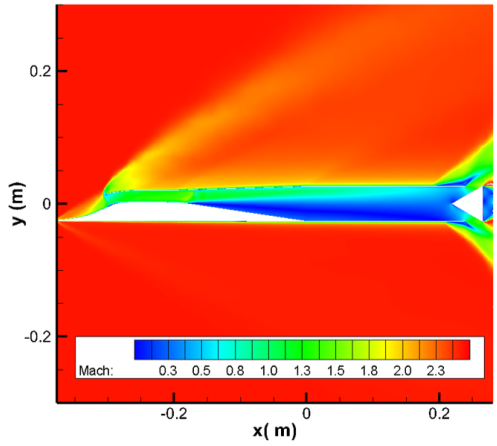

Fig. 3 Contour of Mach number in the inlet without any plasma actuators.

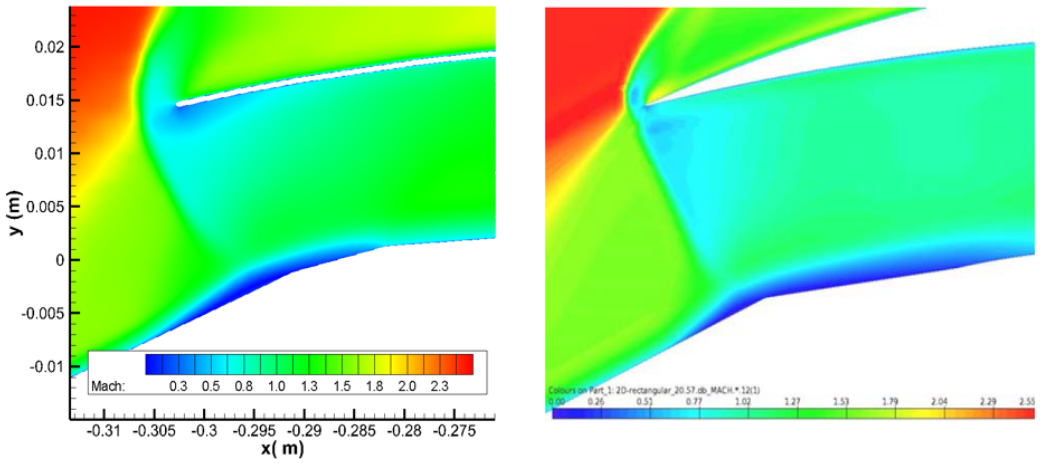

(a) (b)

Fig. 4 Developing separation boundary layer on the ramp at the beginning of the inlet (a) obtained using Fluent and (b) described by Ref. [12]. Differences are mostly attributed to the coarser mesh used as compared to Ref. [12].

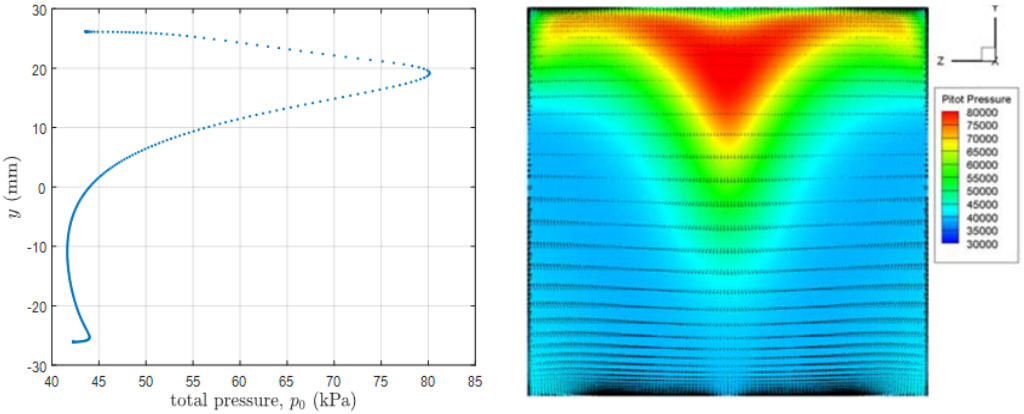

(a) (b)

Fig. 5 Total pressure profile generated at the end of the inlet from (a) the 2D Fluent results and (b) 3D CFD results described in Ref. [12].

Thus, due to lack of SBLI management, the pressure profile at the combustor shows high total pressure distortion and low total pressure recovery which may lead to significant performance loss and increased instability for the airbreathing engine. Table 3 shows the performance parameters calculated at the end of the inlet compared against 3D CFD and experimental results obtained by the Defence Research and Development Canada (DRDC) research agency in [12]. Percent discrepancies from the experimental results are shown in parentheses for the CFD results which demonstrate reasonable agreement with experimental results. The larger percent discrepancy in the pressure distortion is mostly attributed to the missing dimension in the 2D CFD simulations.

Table 3 Performance Parameters at the End of the Inlet Without Plasma Actuators

Performance Parameter	2D CFD	DRDC 3D CFD	Experimental Results
Mass Flow Rate (kg/s)	0.168 (-1.2%)	0.166 (-2.4%)	0.170
Pressure Recovery (%)	74.60 (+5.7%)	60.88 (-13.7%)	70.57
Pressure Distortion (%)	51.64 (+2.5%)	49.82 (-1.2%)	50.40

B. Effects of Plasma Actuator on Inlet Performance Parameters

To establish proper plasma actuator locations and orientations, a total of 80 steady-state simulations were performed using the methodology described in Section III.B. For each simulation, the plasma actuators were centered at one of the three locations shown in Fig. 6. At the locations labelled A and B in Fig. 6, orientations in the positive (coflow) and negative (counterflow) $\hat{x}$ directions and the positive and negative $\hat{y}$ directions were simulated for various actuator strengths. At location C, only coflow and counterflow orientations in the negative $\hat{y}$ direction were simulated.

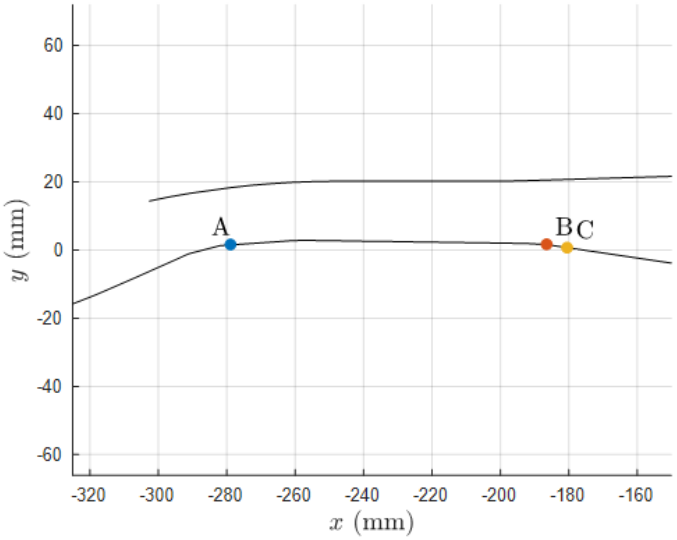

Fig. 6 Locations where the plasma actuators were placed. A corresponds to the center of the bleed block from Ref. [12], B corresponds to the location of flow detachment from the ramp, C is just downstream from B.

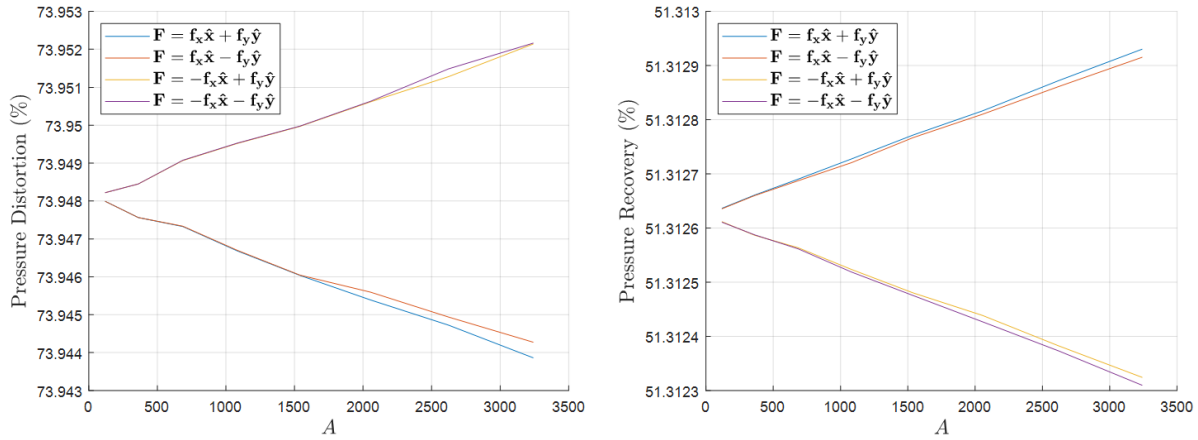

(a)

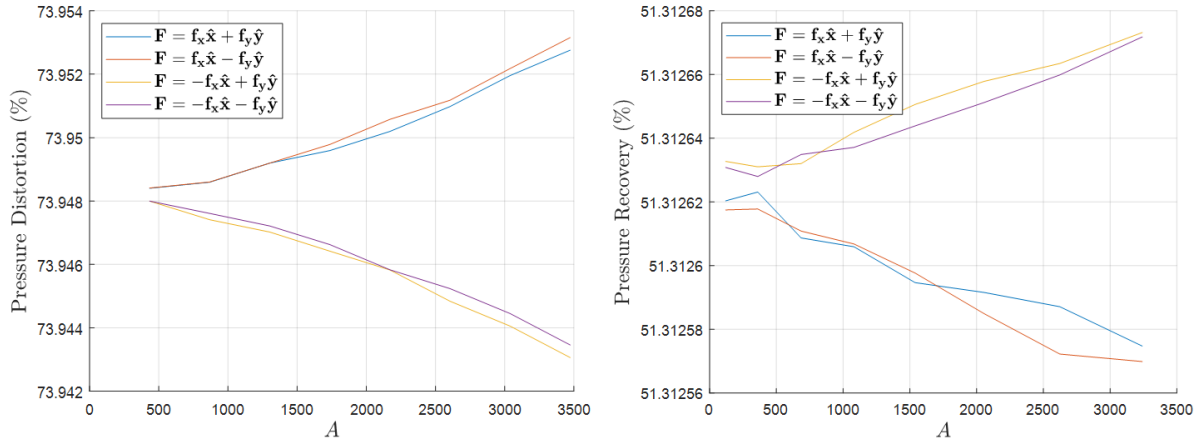

(b)

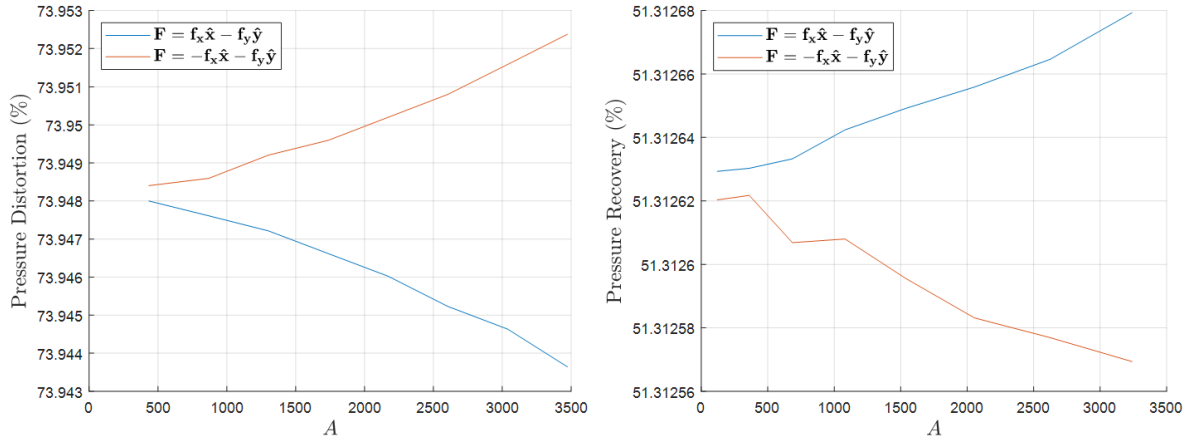

(c)

Fig. 7 Total pressure distortion and total pressure recovery as a function of actuator strength at locations (a) A, (b) B, and (c) C as shown in Fig. 6.

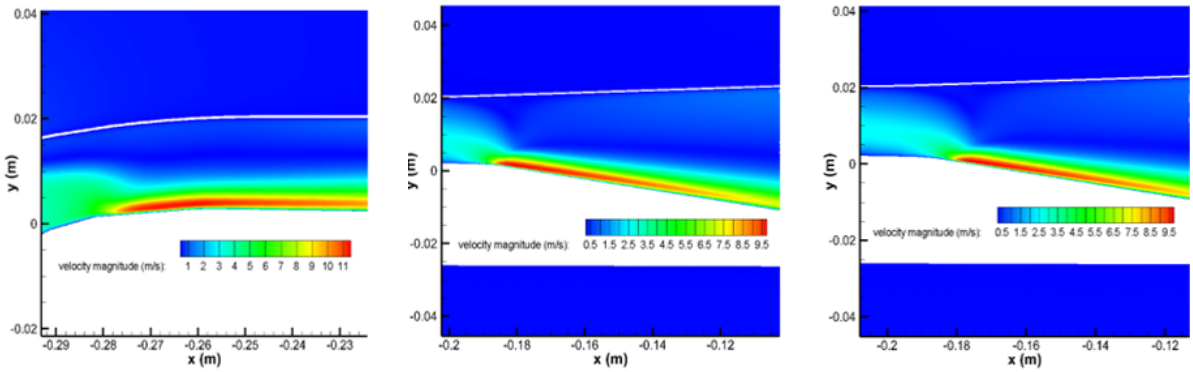

(a) (b) (c)

Fig. 8 Coflow plasma actuators turned to generate a peak velocity magnitude of approximately 10 m/s in quiescent, atmospheric air at locations (a) A, (b) B, and (c) C as shown in Fig. 6. The forcing is tangential to the ramp at the location of the actuator.

Although Fig. 7 demonstrates some influence of the plasma actuators on the performance parameters at the end of the inlet, the overall effect of the plasma actuators on the flow is negligible: the trend for pressure recovery is significant only after the third decimal place and the trend for pressure distortion is significant only after the first decimal place when both are expressed as percentages. However, only small actuator strengths corresponding to approximately 0.5 to 2 m/s max velocity production were tested, partially explaining the small influence on the flow.

Next, transient simulations were performed for coflow, $-f_y$ plasma actuators at locations A, B, and C. A counterflow, $-f_y$ plasma actuator was also simulated at location B. Due to the negligible effects shown in Fig. 7 for small actuator strengths, the forcing function amplitude A was adjusted until the forcing induced a peak velocity magnitude of approximately 10 m/s in quiescent, atmospheric air as shown in Fig. 8. The forcing function amplitude A shown in Fig. 8 corresponds to $A \approx 27,000$.

For all simulations, only approximately 1 sec of flow time was required for changes in the solution to become negligible. Thus after 1 sec flow time, the transient simulations were stopped and the mass flow rate, total pressure recovery, and total pressure distortion at the end of the inlet were calculated for each location as reported in Table 4.

Ultimately, the results demonstrate that even when operating at the maximum induced velocity for most surface DBD actuators at constant forcing [8], the influence on the flow within the inlet from the actuators is very limited. There were no significant changes in the mass flow rate, total pressure distortion, or pressure recovery at the end of the air inlet regardless of the orientation or location of the plasma actuator. The results also demonstrated a decrease in the performance of the inlet, albeit insignificant, for the stronger plasma actuators. The results thus suggest that there may be an optimal configuration that yields the best inlet performance. This remains to be explored in the future.

Ultimately, the results suggest that for surface DBD actuators inducing velocities between 5-10 m/s primarily in the streamwise direction, the standard actuators may not be of sufficient strength to significantly affect the supersonic flow

Table 4 Performance Parameters for Actuators with 10 m/s Peak Induced Velocity at the End of the Inlet

Actuator Location	Orientation	Mass Flow Rate (m/s)	Pressure Distortion (%)	Pressure Recovery (%)
None	N/A	0.168	74.60	51.64
A	Coflow	0.168	74.76	51.64
B	Coflow	0.168	74.72	51.64
B	Counterflow	0.168	74.73	51.64
C	Coflow	0.168	74.67	51.64

in the air inlet. Consequently, future studies should focus on 3D serpentine type actuator geometries which can induce velocities in the spanwise and wall normal direction [15–17], or linear actuators aligned in the spanwise direction.

V. Conclusion

Here, 2D CFD simulation results are presented for the flow control within a supersonic rectangular air inlet using linear surface DBD plasma actuators. A parametric study was performed to identify receptive plasma actuator locations and orientations. Ultimately, the results suggest that in all locations and orientations evaluated, the forcing achieved by current generation linear actuators is negligible for flow control in the inlet when primarily acting in the streamwise direction. However, the results also demonstrate the greatest influence on the performance of the inlet when plasma actuators oriented in the coflow direction are located at the bleed block and the start of the subsonic diffuser in Ref. [12]. Therefore, the work also identifies appropriate actuator locations and orientations where the forcing effects are the most pronounced which can help guide future efforts.

This initial effort was aimed at evaluating the feasibility for supersonic flow control using DBD actuators to improve the performance of supersonic air inlets. As suggested by the present study, future investigation will focus on 3D CFD simulations of 3D actuator geometries which can force in the spanwise direction [15–17]. Numerical simulations may also investigate time-varying, sinusoidal forcing to trip the flow rather than the time-averaged forcing considered in the present work. Different prismatic valve insertion depths may also be investigated.

References

[1] Kim, S. D., "Aerodynamic Design of a Supersonic Inlet with a Parametric Bump," *Journal of Aircraft*, Vol. 46, No. 1, 2009, pp. 198–202.

[2] Arif, I., Salamat, S., Ahmed, M., Qureshi, F., and Irtiza Ali Shah, S., "Comparative Flow Field Analysis of Boundary Layer Diverter Intake and Diverterless Supersonic Intake Configurations," *Journal of Applied Fluid Mechanics*, Vol. 11, 2018, pp. 1125–1131. doi:10.18869/acadpub.jafm.73.247.27928.

[3] Im, S., Do, H., and Cappelli, M. A., "Dielectric barrier discharge control of a turbulent boundary layer in a supersonic flow,"

Applied Physics Letters, Vol. 97, No. 4, 2010, p. 041503. doi:10.1063/1.3473820, URL https://doi.org/10.1063/1.3473820.

[4] Falempin, F., Firsov, A. A., Yarantsev, D. A., Goldfeld, M. A., Timofeev, K., and Leonev, S. B., "Plasma Control of Shock Wave Configuration in Off-Design Mode of M=2 Inlet," *Experiments in Fluids*, Vol. 56, No. 3, 2015, pp. 54–64.

[5] Caraballo, E., Webb, N., Little, J., Kim, J.-H., and Samimy, M., *Supersonic Inlet Flow Control Using Plasma Actuators*, 2009. doi:10.2514/6.2009-924, URL https://arc.aiaa.org/doi/abs/10.2514/6.2009-924.

[6] Leonov, S., Yarantsev, D., and Falempin, F., "Flow control in a supersonic inlet model by electrical discharge," , 2012. doi:10.1051/eucass/201203557, URL https://doi.org/10.1051/eucass/201203557.

[7] Kalra, C., Shneider, M., and R, M., *Numerical Study of Shockwave Induced Boundary Layer Separation Control using Plasma Actuators*, 2012. doi:10.2514/6.2008-1095, URL https://arc.aiaa.org/doi/abs/10.2514/6.2008-1095.

[8] Moreau, E., "Airflow Control by Non-Thermal Plasma Actuators," *Journal of Physics D: Applied Physics*, Vol. 40, No. 3, 2007, pp. 605–636.

[9] Ran, H., and Mavris, D., *Preliminary Design of a 2D Supersonic Inlet to Maximize Total Pressure Recovery*, 2012. doi:10.2514/6.2005-7357, URL https://arc.aiaa.org/doi/abs/10.2514/6.2005-7357.

[10] Whitford, R., *Design for Air Combat*, Janes Information Group, London, 1987.

[11] Kurzke, J., and Halliwell, I., *Inlet Flow Distortion*, Springer International Publishing, Cham, 2018, pp. 249–267. doi:10.1007/978-3-319-75979-1_6, URL https://doi.org/10.1007/978-3-319-75979-1_6.

[12] Moerel, J.-L., Veraar, R., Halswijk, W., Pimentel, R., Corriveau, D., Hamel, N., Lesage, F., and Vos, J., *Internal Flow Characteristics of a Rectangular Ramjet Air Intake*, 2009, pp. 1–26. doi:10.2514/6.2009-5076, URL https://arc.aiaa.org/doi/abs/10.2514/6.2009-5076.

[13] ANSYS® Academic Research CFD, H. S., Release 19.2, "ANSYS Fluent Theory Guide," , 2019.

[14] Singh, K. P., and Roy, S., "Force Approximation for a Plasma Actuator Operating in Atmospheric Air," *Journal of Applied Physics*, Vol. 103, No. 1, 2008, pp. 1–6. doi:10.1063/1.2827484, URL https://doi.org/10.1063/1.2827484.

[15] Gupta, A. D., and Roy, S., "Three-dimensional plasma actuation for faster transition to turbulence," *Journal of Physics D: Applied Physics*, Vol. 50, No. 42, 2017, p. 425201. doi:10.1088/1361-6463/aa8879, URL https://doi.org/10.1088%2F1361-6463%2Faa8879.

[16] Riherd, M., and Roy, S., "Serpentine Geometry Plasma Actuators for Flow Control," *Journal of Applied Physics*, , No. 8, 2013, pp. 1–13. doi:10.1063/1.4818622, URL https://doi.org/10.1063/1.4818622.

[17] Roy, S., and Wang, C.-C., "Bulk flow modification with horseshoe and serpentine plasma actuators," *Journal of Physics D: Applied Physics*, Vol. 42, No. 3, 2008, p. 032004. doi:10.1088/0022-3727/42/3/032004, URL https://doi.org/10.1088%2F0022-3727%2F42%2F3%2F032004.